The use of high resolution numerical simulations of tropical circulation to calibrate stochastic physics schemes

Glenn Shutts and Tim Palmer

European Centre for Medium-Range Weather Forecast
Reading, UK

1. Introduction

Representation of the effects of deep convection in numerical weather prediction (NWP) or climate models is based on an assumed, deterministic relationship between vertical profiles of temperature, humidity and wind and the corresponding vertical fluxes of heat, moisture and momentum. These fluxes can be thought of as a horizontal average over a region containing a very large number of convective clouds. However with observed cloud spacings ranging over tens or even hundreds of kilometers, the corresponding vertical convective fluxes averaged over the scale of an NWP model gridbox will not - at any instant - match the deterministic mean. Furthermore, the size of the averaging area required to include a large number of convective systems may exceed the scale over which environmental conditions are sufficiently uniform to permit a unique relationship between area-mean fluxes and mean profiles of temperature, humidity and wind.

A conceptual way of rationalizing this problem is to imagine a large ensemble of atmospheres whose states, when projected onto an NWP model, are identical but whose sub-grid scale fields are different (i.e. sub-grid clouds are of different sizes and in different places). From this viewpoint one could hypothesize a unique relationship between the vertical profile of ensemble-mean sub-gridscale convective fluxes in any column and their associated model atmospheric profiles. Conventional parametrization schemes based on this hypothesis neglect the effectively unpredictable fluctuations of convective fluxes about the ensemble average. The observed low convective storm population density relative to forecast model grids suggests that the amplitude of these fluctuations could exceed the ensemble-mean value.

Should we be concerned about these statistical fluctuations in the convective mass flux? If the quasi-balanced dynamics of the forecast model does not respond to these relatively high frequency fluctuations then presumably the ensemble-mean parametrized flux would suffice. We know however that mesoscale convective systems on a time scale of less than one day can exert a powerful influence on synoptic-scale flow through the injection of potential vorticity anomalies (e.g. Shutts and Gray, 1994). The short time scale fluctuations associated with convective dynamics can also be expected to excite vertically-propagating internal gravity waves which are able to exert a radiation stress in regions remote from the convective activity and force large-scale flow variability such as the quasi-biennial oscillation (Hamilton, 1998). It therefore seems perfectly reasonable to introduce stochastic fluctuations into the parametrization schemes of NWP and climate models and one might suppose that the performance of these schemes (with respect to systematic error reduction) could even be improved (Palmer, 2001).

A separate, though not entirely distinct issue is the question an upscale kinetic energy cascade that follows the release of kinetic energy in the atmospheric mesoscales. Figure 1 shows the two-dimensional energy spectrum function derived from a high resolution ECMWF 10-day forecast (T799) plotted as a function of the spherical harmonic order n with a logarithmic scale for both axes. The kinetic energy spectrum decomposed into rotational and divergent wind components shows a clear k^{-3} form in the rotational wind and $k^{-5/3}$ behaviour in the divergent wind. The total kinetic energy is dominated by the rotational wind component and this -3 spectral slope is consistent with the observed slope for wavelengths greater than about

600 km (Nastrom and Gage, 1985). However for scales smaller than this, the observed -5/3 spectral slope of Nastrom and Gage is absent. The spectral truncation of the forecast model permits a minimum wavelength of about 50 km and one might have expected to see some sign of this observed shallower spectral slope. Forecasts without horizontal diffusion are no better and it is likely that the diffusive nature of the semi-Lagrangian advection scheme (dependent on the order of accuracy of the interpolation algorithm) is responsible for damping the shortest waves. Does this underestimate of the mesoscale kinetic energy signal the absence of some important physical process?

Convective parametrization schemes implicitly assume that kinetic energy generated by buoyancy forces is dissipated *in situ* (leaving aside local kinetic sources and sinks associated with convective momentum transport and geostrophic adjustment that accompanies subsidence warming). In reality some of this released kinetic energy is radiated as gravity waves and some is retained in quasi-balanced motions (Shutts and Gray, 1994). Other sources of kinetic energy dissipation in the forecast model such as mountain drag and frontal diffusion may also imply levels of turbulent energy dissipation that are not found in reality due to their quasi-two-dimensional nature. By analogy with common practice in Large Eddy Simulation (LES) a possible solution is to stochastically backscatter a certain fraction of this notional sub-gridscale kinetic energy back to the resolved near-grid scales (Mason and Thomson, 1992).

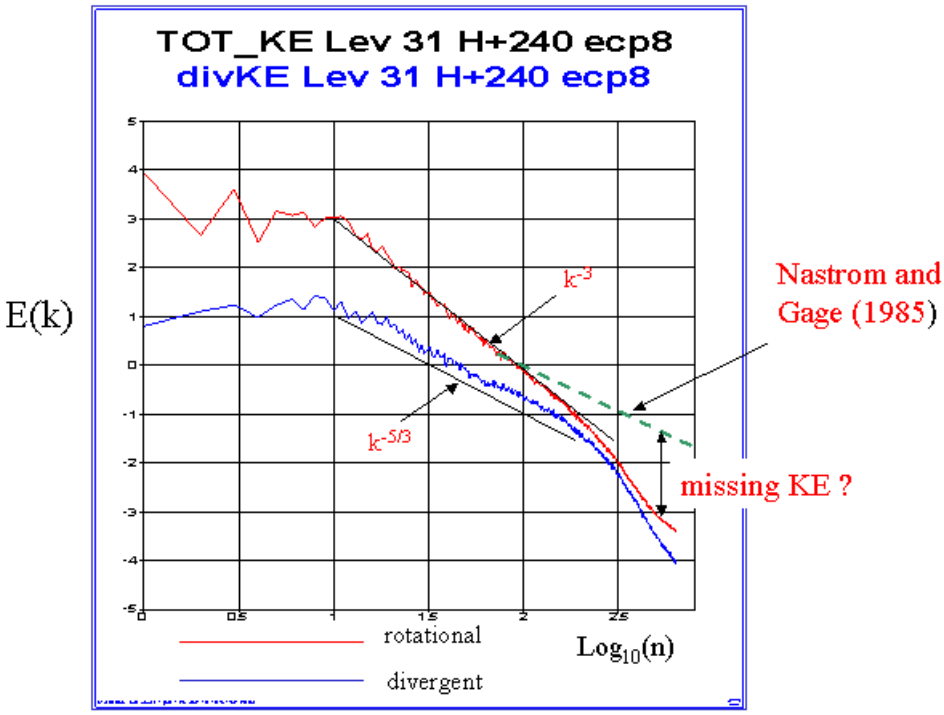

Figure 1 Kinetic energy spectra from a T799 forecast decomposed into rotational and divergent wind components. The green dashed line indicates the observed spectral slope as found by Nastrom and Gage (1985). The discrepancy between model and observations is suggested by the vertical double arrow-headed line.

The purpose of this paper is to summarize some numerical simulations of deep convection in the tropics using a cloud-resolving model (CRM). The convective forcing is computed from coarse-grained fields and its associated statistical properties are characterized by probability distribution functions (pdfs). Similar pdfs have been computed from the ECMWF forecast model system (the IFS) with a view to exposing a potential lack of near-grid scale variability resulting from the omission of stochastic variability in the convective parametrization scheme. The model runs are integrated for about one month giving enough time for low frequency variability of the sort characterizing the Madden-Julian oscillation (MJO) to evolve. With a short,

variable time step (typically about 5 or 6 seconds) and nearly 42 million model points, the computational resource for such simulations is quite substantial.

2. Model configuration for the tropical atmosphere

Numerical simulations are carried out with a modified form of the Met Office 'Large Eddy Model' which is a cloud-resolving model based on the anelastic, quasi-Boussinesq equations of motion (see Shutts and Gray, 1994 for details of the model formulation). The model is configured for three-phase cloud microphysics with separate prognostic variables for water vapour, liquid water and ice cloud, rain, snow and graupel. Numerical advection is based on the 'ULTIMATE' scheme of Leonard et al (1993) for thermodynamic variables and the centred scheme of Piacsek-Williams (1970) for momentum. The model uses bulk surface flux formulae and Smagorinsky-Lilly diffusion (based on similarity theory) to describe boundary layer fluxes of heat, moisture and momentum. Radiative forcing is represented by a prescribed vertical cooling rate profile (typically 1.5 K/day in the troposphere) combined with weak Newtonian relaxation to the initial temperature profile with a timescale of 5.6 days.

A novel feature of the model configuration is the use of an equatorial beta-plane together with anisotropic grid spacing in the horizontal plane. The standard experiment uses a cloud-resolving model gridlength in the zonal direction ($\Delta x = 1$ or 2 km) and operational NWP model resolution in the meridional direction ($\Delta y = 40$ km). In order to span about one quarter of the tropics the horizontal grid is composed of 8192 x 128 points when $\Delta x = 1$ km and 4096 x 128 points when $\Delta x = 2$ km. The 128 points in the meridional direction span a distance of 5120 km corresponding to a latitudinal range of about ± 23 degrees. Although the model domain is somewhat limited in north-south extent it is helpful to the realism of the model to include a Trade wind forcing function in the momentum equation. This works by specifying a basic state geostrophic wind $U_g(y) = -10\cos^2(\pi y / L)$ m/s for the range $-L/2 \le y \le L/2$ (where L is the domain width) and appears as an additional meridional pressure gradient term in the y-component of the momentum equation.

Finally, the model's lower surface is considered to be sea with two different idealizations of tropical sea surface temperature (SST) distribution being used in the simulations; a zonally-symmetric distribution Fig. 2 (a) and a warm pool/cold pool distribution, Fig. 2(b). The zonally symmetric SST run has $\Delta x = 1$ km and the asymmetric SST run uses $\Delta x = 2$ km.

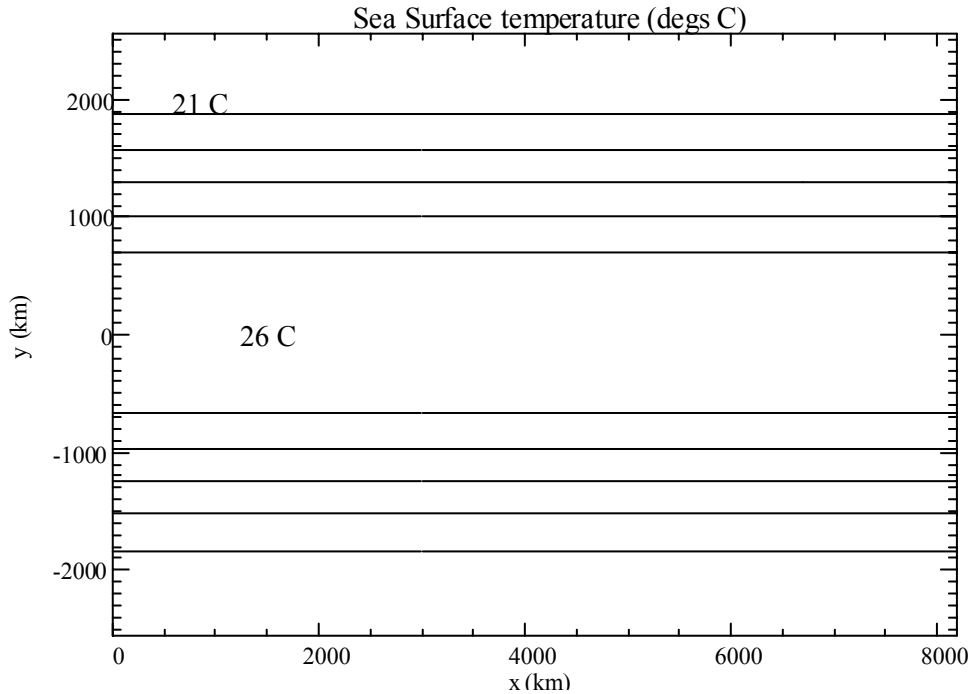

Figure 2 (a) Zonally-symmetric SST distribution used in the run with dx= 1 km. Contour interval: 1 C

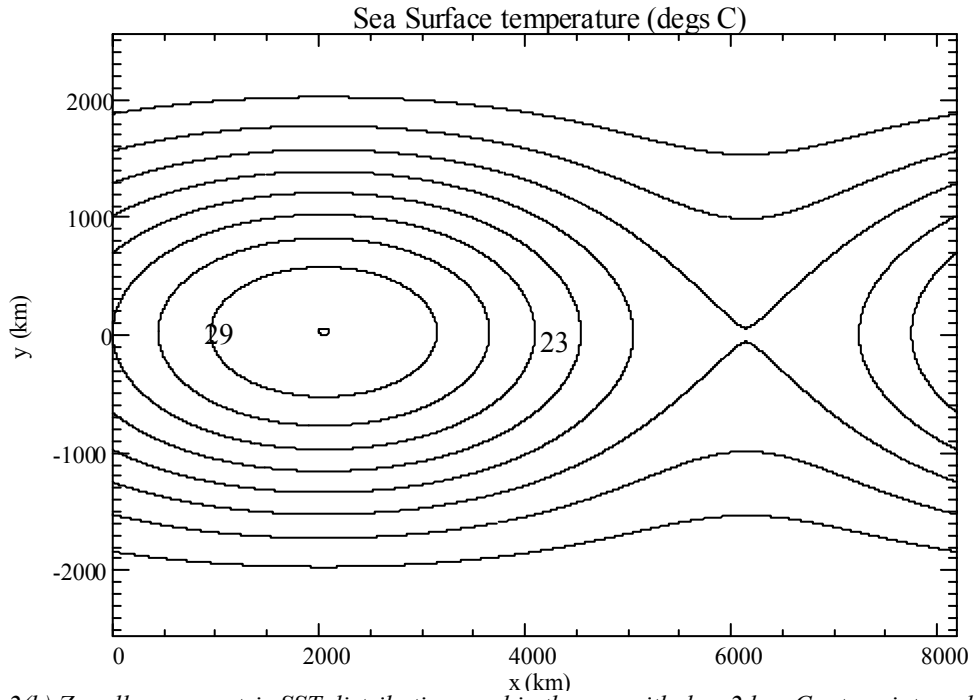

Figure 2(b) Zonally-asymmetric SST distribution used in the run with dx= 2 km. Contour interval: 1C.

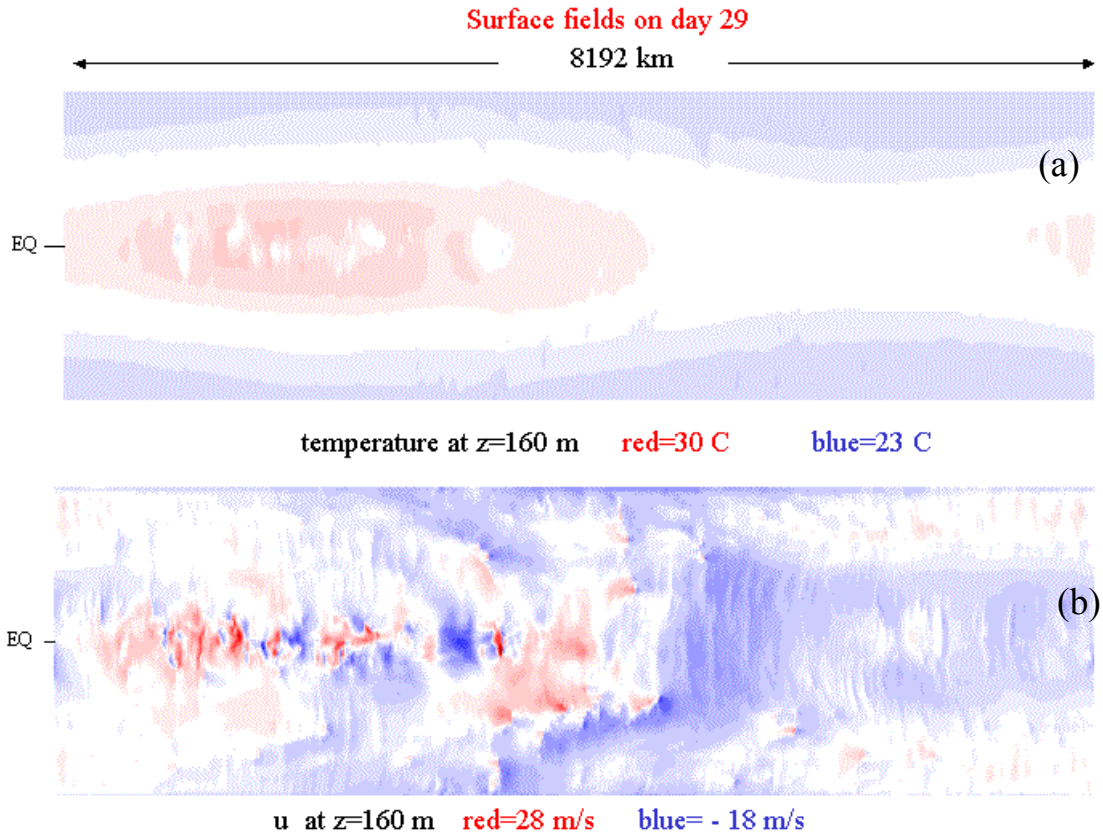

Figure 3 (a) temperature at z= 160 m; (b) u at z=160 m on day 29 of the simulation with zonally-asymmetric SST.

3. Simulated tropical flow – some results

3.1. Overview of the numerical simulations

The combination of high SST and frictional mass convergence near the equator drives deep convection in the model which in view of the grid anisotropy, generates squall line systems oriented in the north-south direction. Figs. 3 (a) and (b) show the boundary layer temperature and zonal wind in the run with the zonally asymmetric SST pattern. The temperature field is similar to the SST pattern except for the presence of cool pools associated with convective downdraughts.

Locally two-dimensional convective systems therefore tend to develop in the xz-plane but not in the meridional direction. Even so, the squall line convection that does develop is found to have fairly limited north-south extent (e.g. 200 to 800 km) and unlike a two-dimensional model can radiate and advect energy meridionally. The near-surface zonal wind is generally easterly over the cooler equatorial waters but the disturbed warm SST regions are characterized by westerlies which are locally strong near convective systems.

Figure 4 shows a vertical section through a convective system in the model showing strong westerlies towards a surface convergence zone and an upper level westerly outflow to the east.

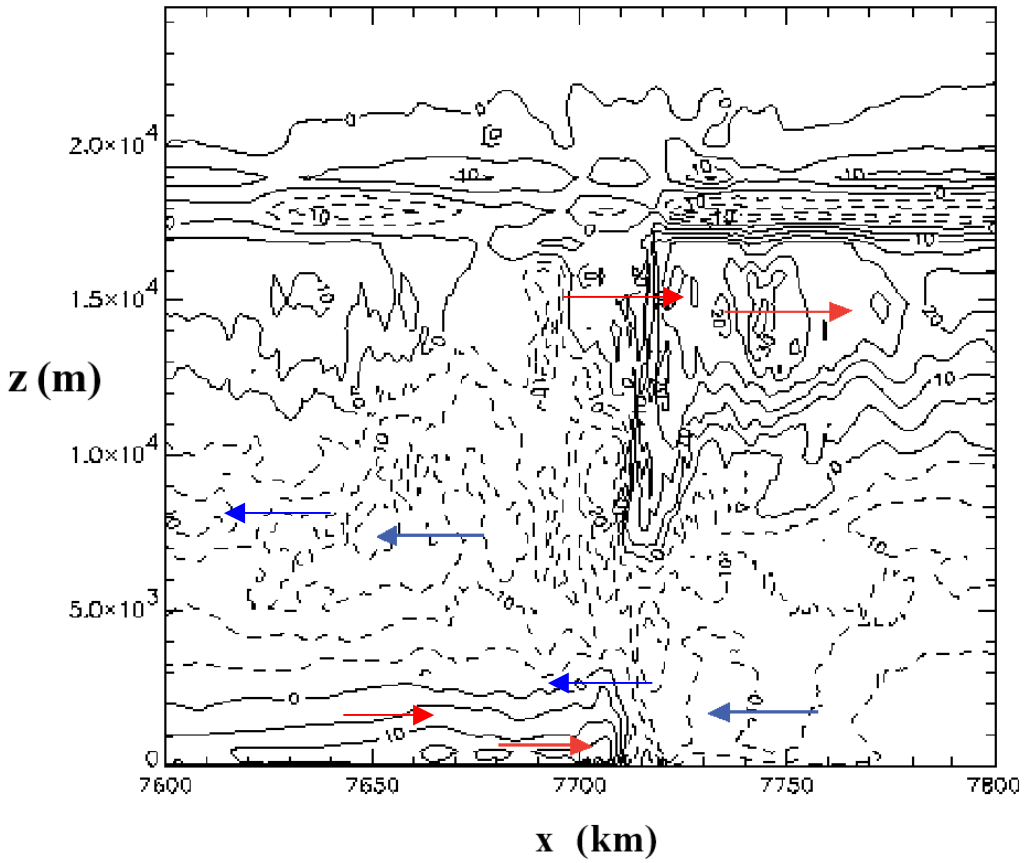

Figure 4 A 200 km long vertical section of u *through a model convective system taken along the equator. Contour interval: 5 m/s.*

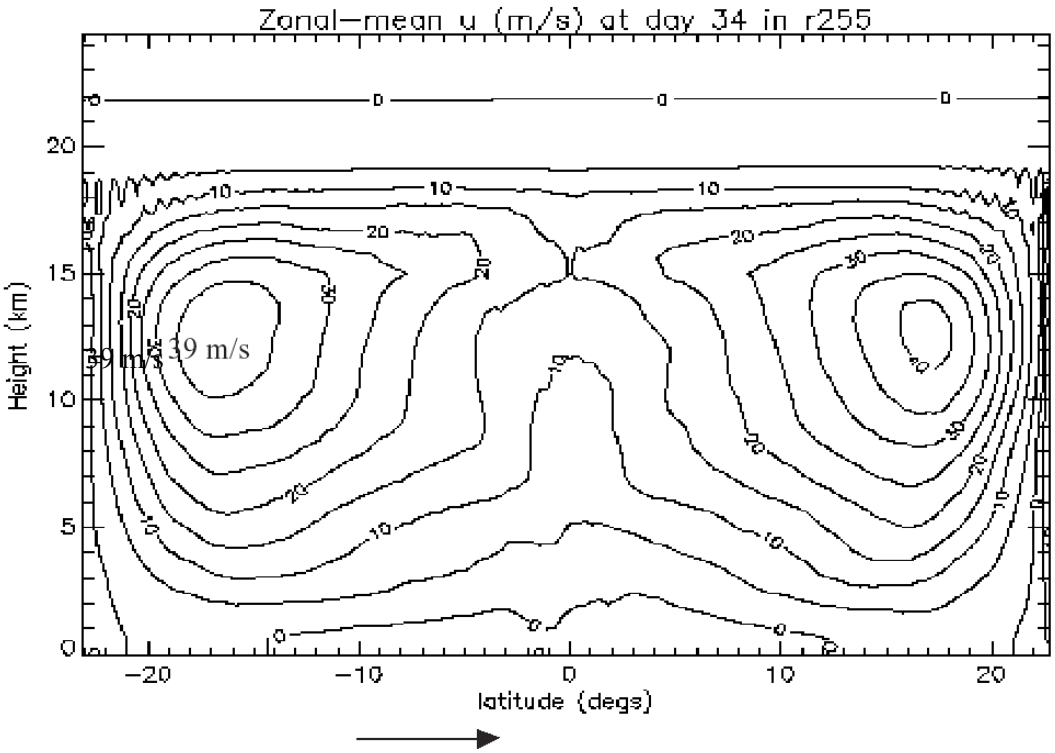

Figure 5 Zonally-averaged u in yz-section at day 34 in the run with zonally-asymmetric SST. Contour interval: 5 m/s

The warmth associated with the meridional variation in surface temperature is transmitted to the atmosphere by convection and the resulting thermal wind adjustment leads to westerly wind shear through most of the domain with upper jets forming towards the northern and southern edges of the domain (Figure 5). The position of these jets is equatorward of the observed subtropical jetstreams though their strength is not unrealistic.

Although convection breaks out fairly uniformly in longitude to begin with it soon becomes organized at progressively longer zonal scales and propagates eastward. This is conveniently represented by a Hovmuller diagram of the surface rainfall rate (averaged between 10 N and 10 S): figures 6 and 7 show such plots for the zonally symmetric and asymmetric SST runs respectively. In Figure 6 the convection is organized into clusters that propagate eastwards initially at 10 m/s but later at about 20 m/s. Within each convective cluster, individual convective cells travel westward and some of these precipitation lines on the Hovmuller diagram appear to continue over from one convective cluster to the next, *through the intervening dry zones*.

In the run with a warm SST pool on the western side of the domain the Hovmuller diagram (Figure 7) shows an initial burst of convection that transfer slowly eastwards over a period of two weeks. Convective clusters within the active region propagate eastwards at about 5 m/s. Further into the simulation these eastward propagating clusters move at speeds of about 10 m/s but, in contrast to the zonally-symmetric SST run, develop westward propagating clusters travelling at about -5 to -10 m/s on the 'warm side' of the domain.

No attempt has been made to determine the nature of these propagating clusters but it seems likely that the eastward propagating clusters are linked to Kelvin waves and the westward propagating systems may be of the equatorially-trapped Rossby wave variety. The eastward propagating clusters fall into the category of `MJO-like' disturbances: in common with similar modelling studies (e.g. Grabowski and Moncrieff, 2001) the speed of propagation of the convective clusters is faster than that associated with the MJO.

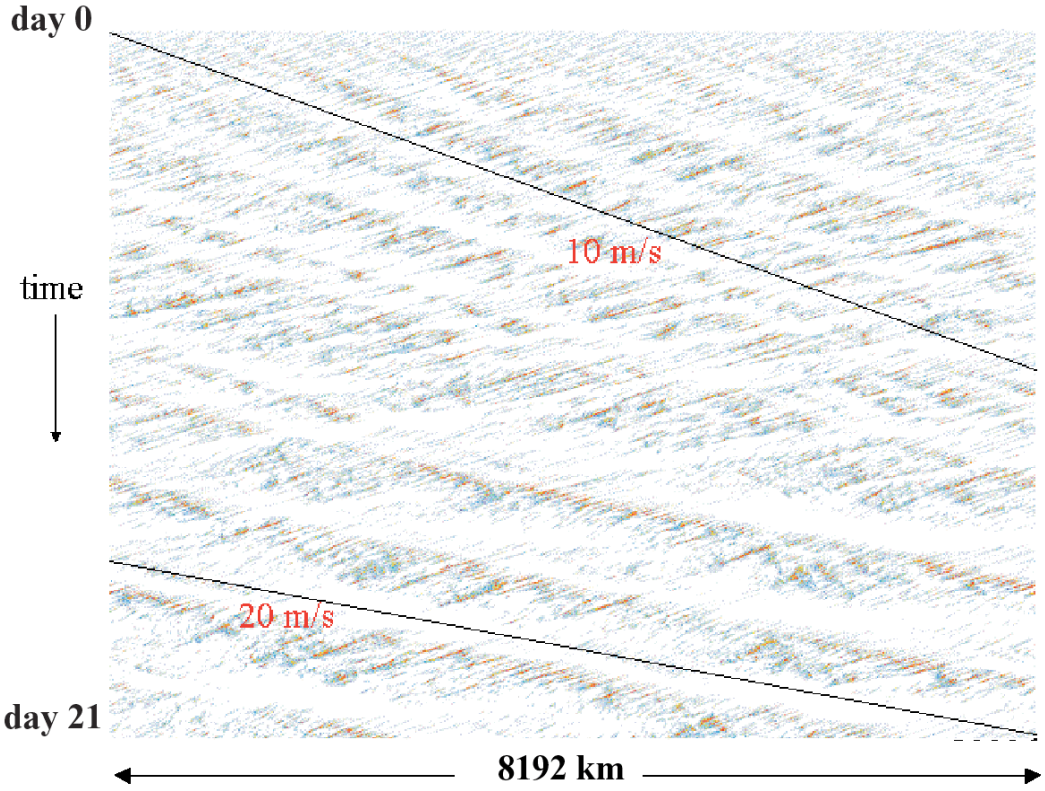

Figure 6 Hovmuller diagram showing the surface precipitation rate averaged between 10 degrees north and south over 21 days in the run with zonally-symmetric SST ($\Delta x = 1$ km; red equals 100 mm/day)

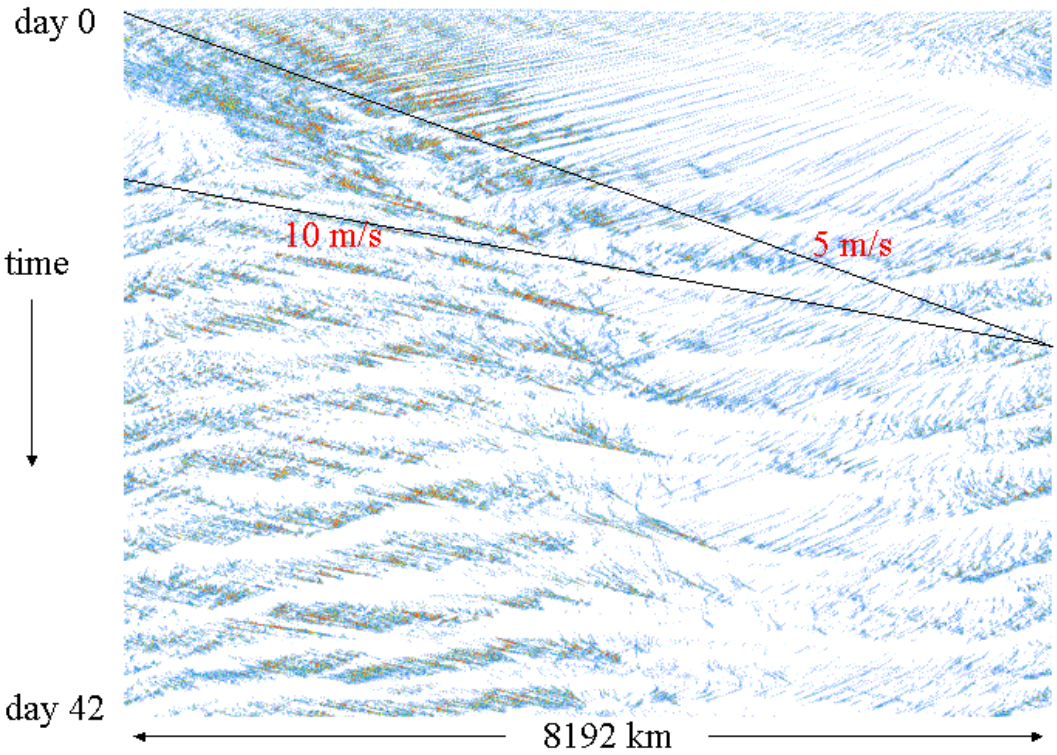

Figure 7 Hovmuller diagram showing the surface precipitation rate averaged between 10 degrees north and south over 42 days in the run with zonally-asymmetric SST ($\Delta x = 2$ km; red equals 100 mm/day)

Because of the equatorial beta-plane geometry and SST field orientation, the computational problem is not invariant to 90-degree rotations and one might question the choice of grid anisotropy used here. Specifically, what is the effect of using high resolution in the y-direction and coarse resolution in *x*? To address this issue a third numerical simulation (with zonally-symmetric SST) has been performed using $\Delta x = 40$ km and $\Delta y = 1.5$ km with 256 points in the x direction and 4096 points in the *y* direction. This choice implies a domain size of 10,240 km x 6144 km i.e. slightly larger than the other two simulations. Figure 8 shows the resulting Hovmuller diagram for surface rainfall rate up to day 16.7. The simulation

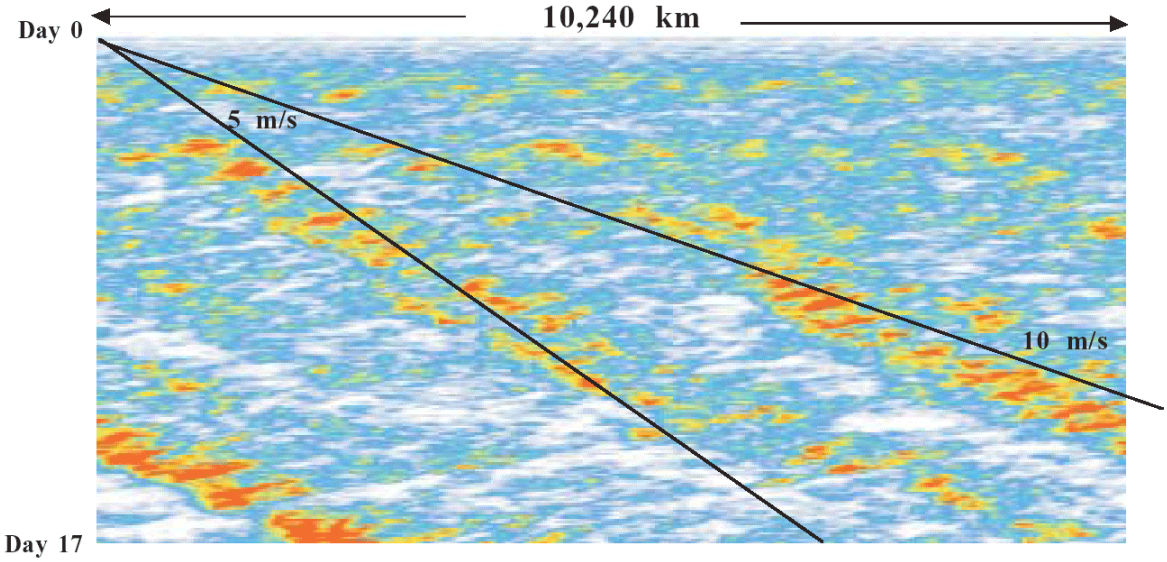

Figure 8 Hovmuller diagram of surface precipitation rate averaged between 10 degrees north and south in a run with high resolution in y ($\Delta x = 40$ km, $\Delta y = 1.5$ km; white=0, red= 35 mm/day). The time scale extends from 0 to 16.7 days and the two solid lines represent the paths of features travelling eastwards at 5 and 10 m/s from x=0.

begins with a fairly prominent zonally symmetric oscillation but after about 4 days this gives way to eastward propagating convective clusters with 3000 km separation. Their propagation speed is about 5 to 7 m/s i.e. noticeably slower than in the corresponding simulation with high resolution in *x*. In this respect they are similar to the eastward propagating convective super-clusters of the Madden-Julian oscillation though it is not immediately obvious why high meridional resolution should favour their simulation over zonal resolution.

3.2. Statistics of convective forcing

From a numerical weather prediction context we would like to establish how the statistics of convective forcing, averaged to the model's grid scale, depend on the local vertical profile of wind, temperature and humidity. Here we are concerned with the magnitude of the fluctuations about the mean rather than the convective parametrization problem *per se*. These convective forcing statistics will be used to calibrate stochastic convective parametrizations, or at the very least provide a plausibility check on their properties. The strategy used to quantify convective forcing in the numerical model is to coarse-grain the model fields to a grid of similar resolution to an operational NWP model. Figure 9 illustrates the relationship between the model gridboxes and the coarse grid with each coarse gridbox containing a 64 x 2 block of model gridboxes.

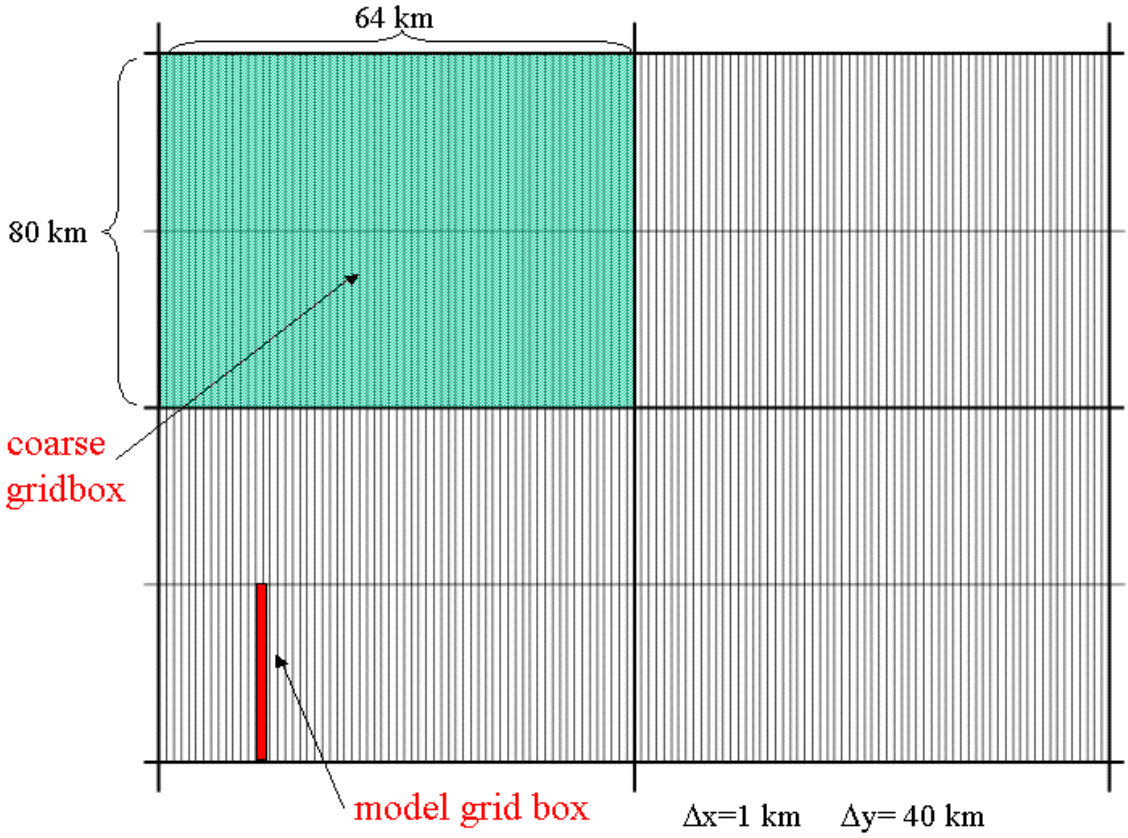

Figure 9 Coarse-graining of the model fields is achieved by averaging model gridbox values (red) over the coarse gridbox rectangles (green). In this illustration there are 128 model gridboxes within each coarse gridbox.

Consider now the thermodynamic equation:

$$\frac{\partial \theta}{\partial t} + V.\nabla\theta = D \qquad (1)$$

where θ is the potential temperature, V is the wind vector and D represents all diabatic source terms (e.g. latent heat release). Denoting the average over each coarse gridbox region by an overbar, eq.(1) averaged to the coarse grid can be expressed as:

$$\frac{\partial \overline{\theta}}{\partial t} = \overline{D} - \overline{\left(V \cdot \nabla \theta\right)}$$

and, adding $\overline{V} \cdot \nabla \overline{\theta}$ to both sides gives:

$$\frac{\partial \overline{\theta}}{\partial t} + \overline{V} \cdot \nabla \overline{\theta} = \overline{D} + \overline{V} \cdot \nabla \overline{\theta} - \overline{\left(V \cdot \nabla \theta\right)} = \hat{Q}_1 \tag{2}$$

where the right-hand side $(\hat{Q}_1)$ represents the net diabatic forcing seen by the coarse-grained flow. This apparent warming/cooling includes those terms used to define Q_1 (the temperature tendency of convective parametrization) but has in addition, contributions from the horizontal eddy heat flux divergence and diffusion. Our interest is focused on the statistical character of $\hat{Q}_1$ and its comparison with the corresponding term in a forecast model. For this purpose the radiative contribution is removed.

Figure 10 shows the probability distribution functions for $\hat{Q}_1$ at two different heights in the model (1 km and 5 km) and for two coarse gridbox sizes (64 km x 80 km and 512 km x 640 km). The pdfs are fairly symmetric about a small positive value with smaller variance at a height of 1 km and also for the larger averaging area (as one might have expected intuitively since the larger averaging area contains more convective clouds). In contrast, pdfs of Q_1 drawn from a similar level in the IFS show a high degree of asymmetry with the majority of gridpoints experiencing a warming (Figure 11a). Using the coarse-grained cloud-resolving model fields as input to a convection parametrization (in this instance, for reasons of convenience, the scheme of Bechtold et al, 2001) one can compute an associated Q_1 field, referred to here as $\widetilde{Q}_1$. The pdf of this derived field will provide some statistical information about the range of thermodynamic profiles and convective instability to be found in CRM grid columns (Figure 11b). Comparison with Figure 11a shows that the cloud-resolving models pdf is similar in form to that derived from the forecast model though with generally higher proportion of gridpoints within each bin (except the one containing $\widetilde{Q}_1 = 0$, i.e. there are fewer convectively stable grid columns in the CRM).

The symmetry of the $\hat{Q}_1$ pdf and the accompanying negative values are likely to be symptoms of averaging over too small an area so that the passage of individual convective squall lines through the coarse grid leads to advective tendencies which rise and fall locally. Regular gravity waves propagating horizontally will also generate a symmetrical spread of tendencies about zero and so some caution is required in the interpretation of these results. Nevertheless, if the CRM has a sufficiently realistic description of tropical convection, the differing pdf of the forecast model supports the idea that there is a lack of variability in the near-gridscale cloud forcing.

If the averaging area is increased to 1024 km x 1280 km, the pdf of $\widetilde{Q}_1$ at a height of 5 km is substantially asymmetric and similar to the pdf of Q_1 derived from the IFS (Figure 12). This is consistent with the reduced contributions of advective effects (associated with the passage of individual cloud systems) and horizontal eddy heat flux divergence.

The coarse-graining technique has also been applied to the x component of the momentum equation and the resultant convective momentum forcing on the coarse grid is compared with the convective momentum source (QU) derived from the IFS's parametrization scheme. Figure 13 shows the pdf of QU at a height of 4.9 km in the forecast model and should be compared with the corresponding pdf of the apparent momentum source computed from CRM fields (Figure 14). The Coriolis and pressure gradient forces are not included in this coarse-grained momentum source. It appears that the CRM simulation experiences much larger fluctuations in momentum forcing at the coarse grid scale than those driven by the convective parametrization scheme in the IFS.

Pdfs of Q_1 from the IFS indirectly represent the range of convective stabilities found within the tropics and since the parametrization provides a unique profile of Q_1 for a specific atmospheric column state, they could be used to classify different synoptic environments. However for any real atmospheric profile, the profile of convective warming could be expected to fluctuate about the mean according to a different characteristic pdf.

Therefore, the CRM pdfs dealt with so far can be decomposed into two distinct components. To isolate the component associated with statistical fluctuation given a particular environmental stability one can bin the $\hat{Q}_1$ values into specific ranges of $\tilde{Q}_1$. Figure 15 shows a preliminary attempt to carry out this decomposition based on 7 consecutive, horizontal fields at daily intervals.

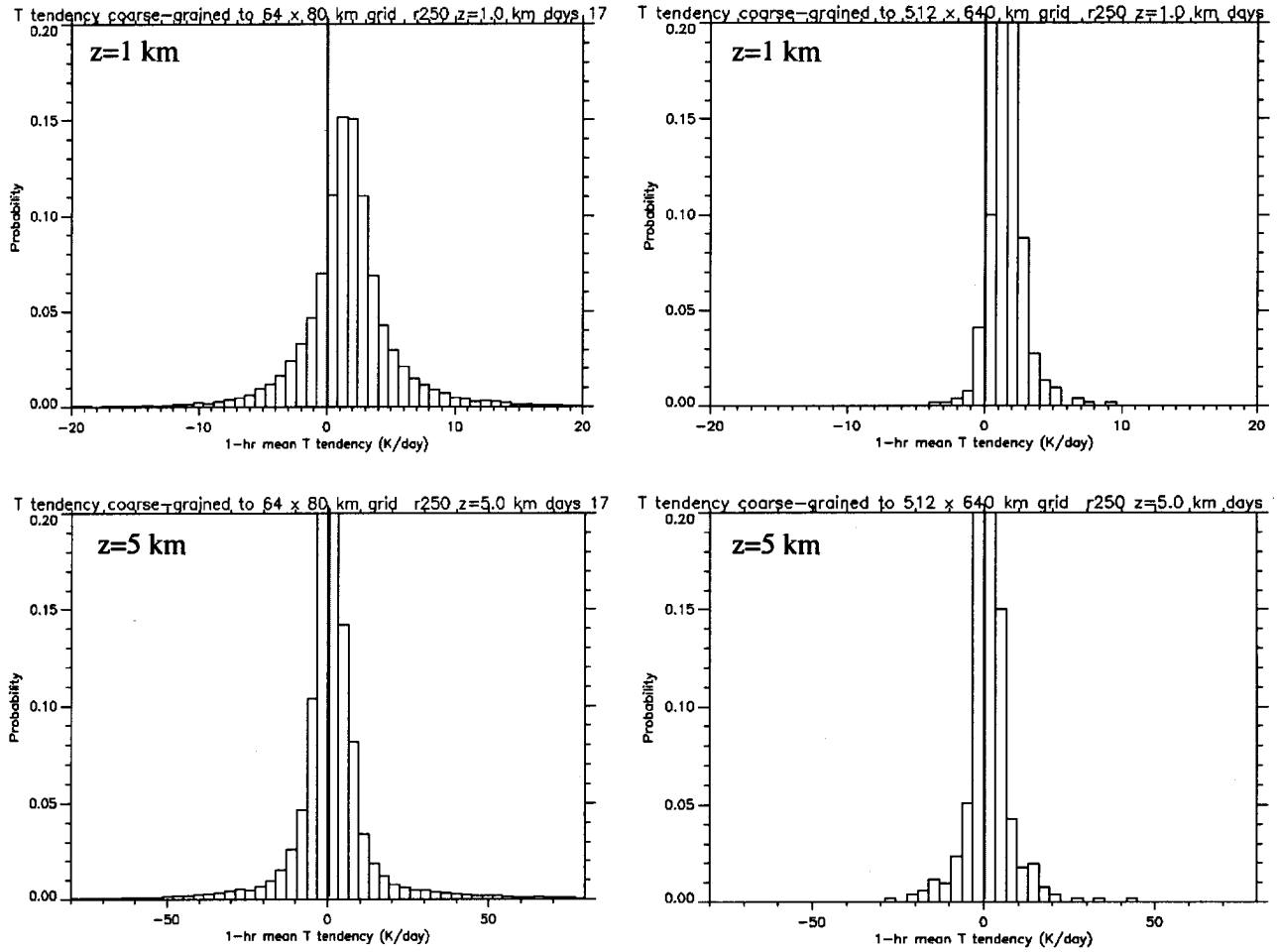

Figure 10 Probability distributions of the apparent heating rate on coarse-grained grids. The left hand figures are for coarse gridboxes of dimensions 64x80 km and the right-hand figures are for coarse gridboxes of 512x640 km. The upper figure pdfs are computed at z= 1 km and the lower figures at z= 5 km.

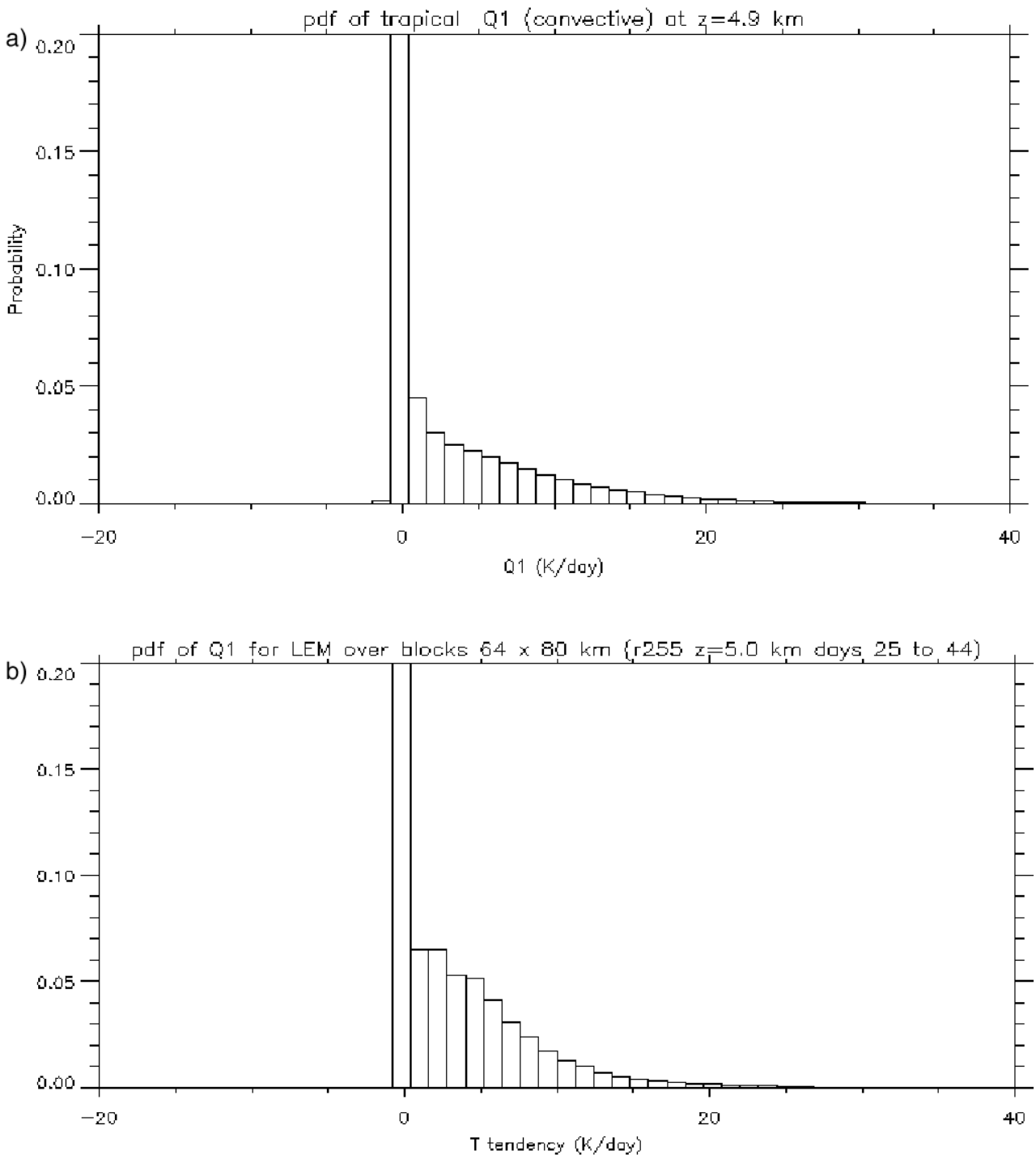

Figure 11 (a) Pdf of the apparent heating Q1 in the ECMWF forecast model due to convective parametrization at z= 4.9 km ; (b) pdf of $\tilde{Q}_1$ obtained by using the coarse-grained fields as input to a convective parametrization scheme.

Each $\hat{Q}_1$ field comprises 8192 x 128 points derived from 1-hour mean winds and temperatures. In spite of the large number of data points available, it is likely that the means and standard deviations quoted in Figure 15 are subject to some error due to a insufficiently large sample size. Nevertheless it can be seen that there is a trend towards higher means and variances as $\tilde{Q}_1$ increases (note however that the computed mean $\hat{Q}_1$ values do not fall within the corresponding bin range of $\tilde{Q}_1$).

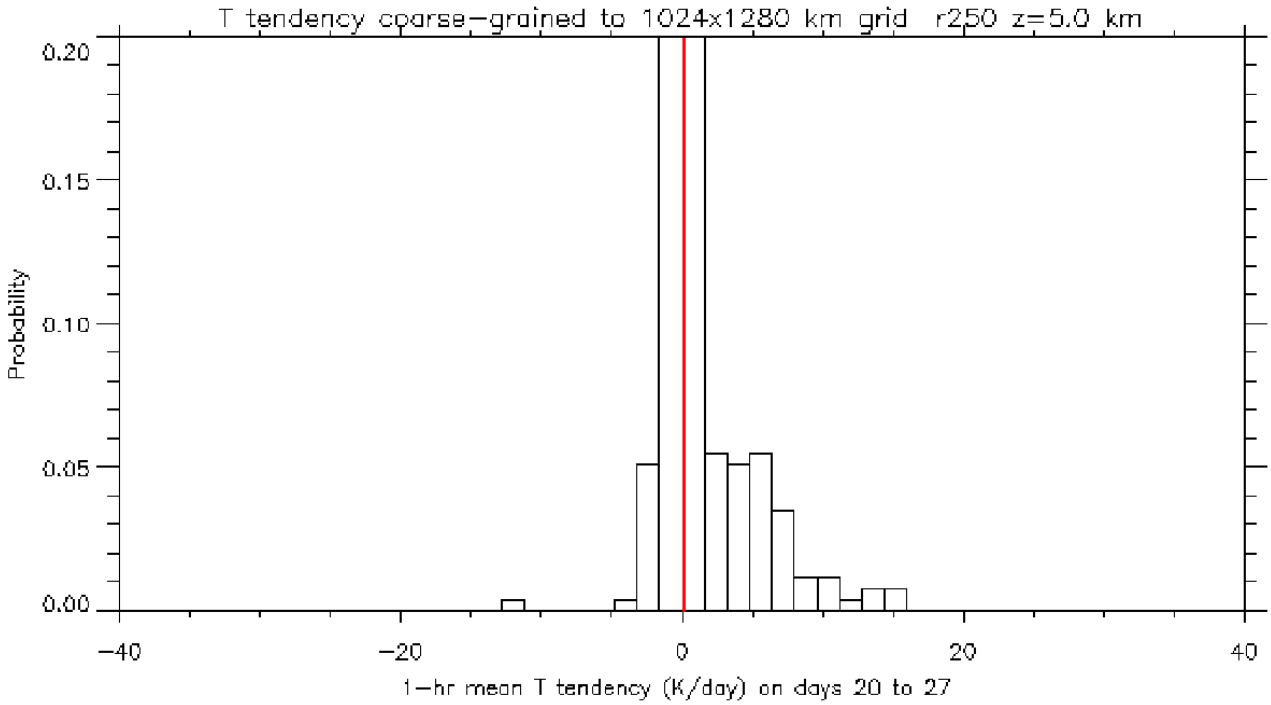

Figure 12 as for the previous figure except coarse-grained to 1024 x 1280 km and from the run with zonally-symmetric SST.

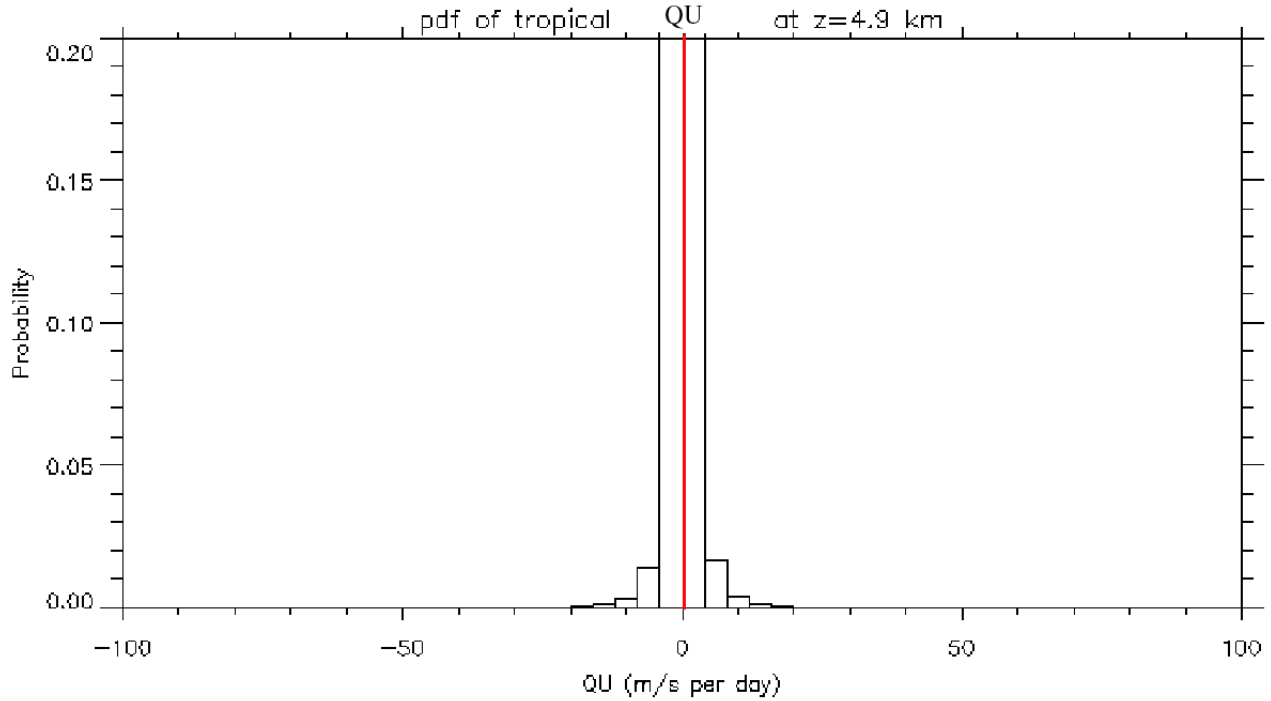

Figure 13 pdf of the convective momentum tendencies (QU) in the IFS at a height of 4.9 km.

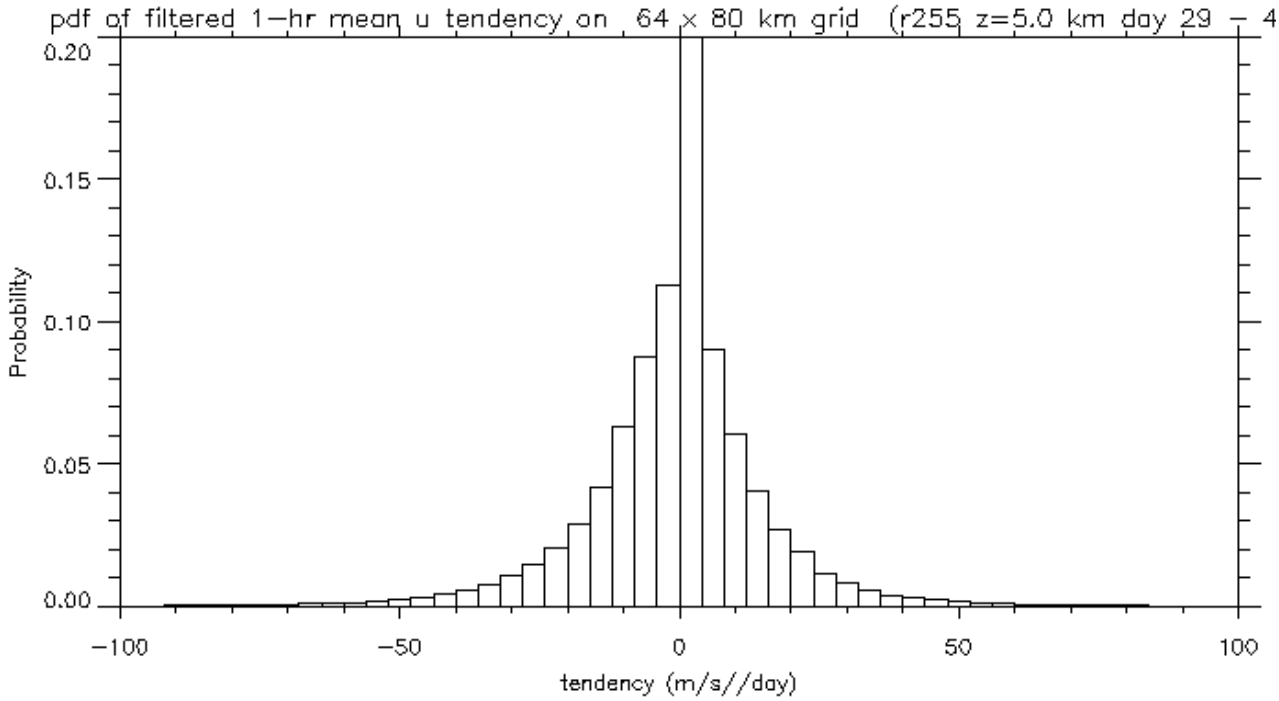

Figure 14 pdf of the apparent tendency of u derived by coarse-graining a sequence of 16 cloud-resolving model fields at

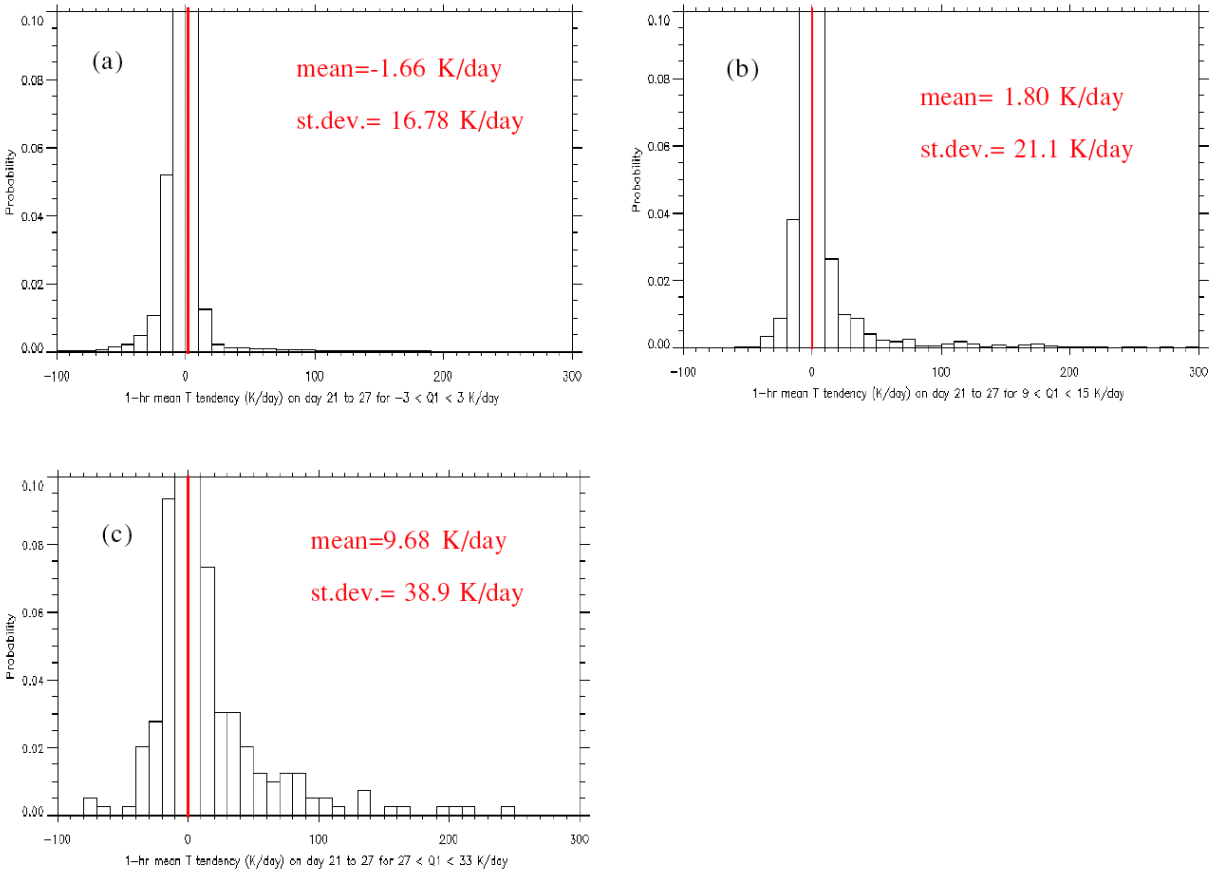

Figure 15 pdfs of apparent temperature tendencies $\tilde{Q}_1$ binned into three levels of convective forcing, $\tilde{Q}_1$ (a) -3 to +3 K/day; (b) +9 to +15 K/day, and (c) +27 to +33 K/day.
The convective forcing strength $\tilde{Q}_1$ is computed by using the coarse-grained model fields as input to a convective parametrization scheme. The pdfs are derived from sub-samples of all model points at z= 5km selected according to the indicated ranges of $\tilde{Q}_1$.

3.3. Stochastic forcing model based on a cellular automaton

Experiments have been conducted in which the previously described cloud-resolving simulations have been repeated with nearly uniform coarse horizontal resolution. In the two experiments to be described $\Delta x = 32$ km and $\Delta y = 40$ km with 256 x 128 gridpoints covering a region 8192 km x 5120 km. At this resolution it is essential to use a convective parametrization scheme (Bechtold et al, 2001) to maintain gridscale convective stability. In this framework, the possible beneficial effects of stochastic perturbations to parametrized tendencies can be tested with the cloud-resolving runs serving as 'truth'.

Rather than use a random number generator indiscriminately to perturb tendencies at the gridpoint level, a pattern generator is formulated from a cellular automaton (CA) and used to drive tendency perturbations with spatial and temporal coherence. The CA was developed as an extension to a well-known family of cellular automata called 'Generations' which add cell history to the prototype 'Game of Life' ruleset. As a very simple illustration of how a CA works consider the cell array depicted in Figure 16. Here, each cell may be alive (red) or dead (white) and the state of the cells at the next step is governed by rules that involve their eight neighbours (referred to as the *neighbourhood*). A living cell will survive to the next step if it has either 2 or 3 living neighbours and a dead cell will remain dead unless it has exactly three living neighbours. Although the change in pattern for this example is unremarkable, complex and interesting pattern evolution is readily found for quite simple survival and birth rules (Wolfram, 2002).

The CA developed here for use in stochastic physics schemes was selected for the similarity of the pattern evolution to certain fields in CRM simulations (e.g. boundary layer temperature beneath a field of deep convective clouds). In it, each cell has 32 lives and is subject to the following birth and survival rules which count only living cells in the neighbourhood that have not yet lost a life (referred to here as 'fertile cells'. Cell survival requires exactly 3,4 or 5 fertile cells in the neighbourhood and the birth of a new cell requires 2 or 3 in the neighbourhood. Non-fertile cells do not participate in the neighbourhood count but impact on cell survival by limiting the space available for cell birth.

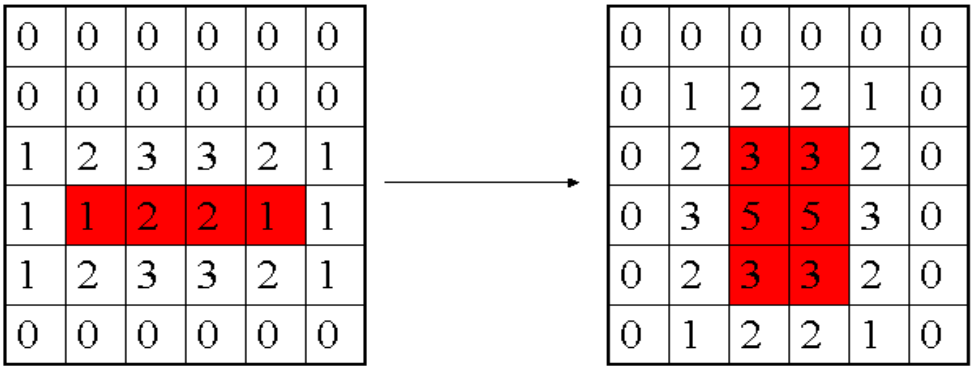

Figure 16 A simple cellular automaton in which cells are either alive (red) or dead (white). The two CA states show a transition based on the survival condition: 2 or 3 living nearest neighbours and the birth condition; 3 living neighbours. The numbers within boxes indicate the number of living nearest neighbours for that cell.

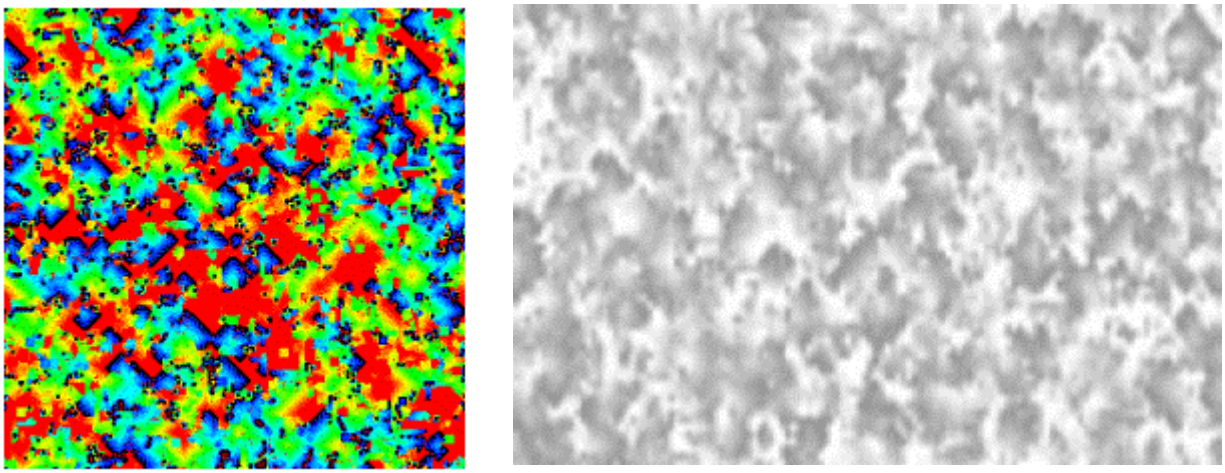

Figure 17 (a) A colour-coded depiction of CA state based on cells that have 32 lives (see text for rule set). (b) an example of a 'weighting function' derived from the CA by coarse-graining, scaling and normalizing the integer-valued CA field.

The CA is started by randomly seeding the grid with new cells and is advanced by 2000 steps to 'spin-up' the pattern. Figure 17 shows a graphical depiction of the integer array that defines a particular CA state. The CA grid is chosen to be 4 times finer than the model grid and is coarse-grained to the model grid, smoothed with a 1-2-1 filter and normalized so that the domain mean is unity. If the resulting field is denoted by $W(x,y,t)$ then the multiplier $\psi = 1 + \alpha(W-1)$ (where α is a constant) is used to modulate the parametrization tendencies in the CRM .

In the experiment featured below the ψ multiplier is applied to the convective parametrization tendencies of T and q with $\alpha = 3$. Figures 18 (a)-(d) show Hovmuller plots of surface precipitation rate and *u* at *850* mb for runs with zonally-symmetric SST, with and without modulated tendencies. The precipitation rate in the control run without perturbed tendencies (Fig. 18a) is quite bland but after a week or so shows evidence of a fast-moving, eastward propagating disturbance. A cursory comparison with the Hovmuller diagram of the CRM simulation (Figure 6) suggests that the model with parametrized convection has failed to capture the structure and intensity of the eastward propagating convective cloud clusters (for a more direct comparison see Figure 19). When the above CA-based tendency pertubations are introduced the variability in precipitation rate is increased with both eastward and westward propagating disturbances modulating the precipitation rate. Overall the eastward disturbances dominate though not to the extent seen in Figure 6. The corresponding zonal wind component plots in Figures 18 (c) and (d) give a similar message with the eastward propagating disturbances forming much earlier when the tendency modulations are included.

The above experiment is just an illustration of a technique and requires careful analysis to quantify the extent to which the CA-based perturbations are beneficial. The methodology employed is an extension of that used in the operational EPS at ECMWF (Buizza et al, 1999) where a uniform tile pattern is defined from random numbers assigned to latitude/longitude boxes for a fixed time interval. The CA provides a way of generating patterns that resemble observed and simulated mesoscale variability in temperature, humidity and cloud. A logical extension of this technique would be to couple the CA to the forecast model's fields. In this way the character of the pattern (e.g. scale of the clusters) would reflect certain environmental properties like CAPE or the depth of the convecting layer. Progress along these lines has already been made by Khouider, Majda and Katsoulakis (2003) who, borrowing from ideas in materials science, coupled the coarse-grained fields from a stochastic spin-flip model to an idealized model of the tropical atmosphere with simple convective parametrization.

In the context of the CA model described here it is possible to treat the number of lives allocated to new cells as a variable (say, *NL*). Figure 20 shows three weighting function fields derived from CA states with differing *NL* parameter *:* the larger *NL*, the larger the scale of the patterns that evolve on the CA grid. It should therefore be possible to mimic the observed dependence of horizontal convective cloud scale on layer depth and CAPE through *NL*. Coarse-graining the CA weighting function field to a forecast model grid would lead to near-gridscale fluctuations that depend on the *NL* parameter e.g. the fluctuations in the field on the left in Figure 20 might average out whereas those in the image on the right might persist by virtue of their larger scale.

4. Summary

Numerical experiments with a cloud-resolving model, configured to span approximately one quarter of the tropics, have been discussed. A novel aspect of these cloud-resolving simulations is the use of an equatorial beta-plane together with a highly anisotropic horizontal grid with grid spacings of order 1 km in one direction and 40 km in the other. Although the experiments were motivated primarily by the need to collect quantitative information regarding the statistical fluctuations of convective forcing at various scales, they are also relevant to the study of the Madden-Julian oscillation and other forms of low frequency variability in the tropics.

The simulation with zonally-symmetric SST and high resolution in the east-west direction evolves eastward-propagating convective cloud clusters within a few days. The dominant zonal wavelength of these expands steadily to reach 4000 km after about 20 days at which time they travel at about 20 m/s. A simulation with high resolution in the meridional rather than zonal direction produces convective cloud clusters with a similar zonal scale yet slower propagation speed (i.e. 7 m/s). In this respect they resemble the slow eastward propagating cloud systems that characterize the Madden-Julian oscillation though the observed phenomenon is more complex.

Preliminary results obtained by coarse-grain averaging the thermodynamic source term and removing the advective tendency of potential temperature associated with the coarse-grained fields gives a measure of the apparent heat source on the coarse grid. Pdfs of this quantity on coarse grids with similar resolution to operational NWP models reveal a degree of symmetry and variance about the mean that is not found in the ECMWF forecast model. The convective parametrization scheme gives generally positive heating tendencies in mid-troposphere and the fluctuations about zero seen in the coarse-grained tendencies are probably dominated by advective contributions graining the fields to gridlengths in excess of 1000 km gives a tendency pdf that better matches those found in the forecast model since individual convective systems lie predominantly within the coarse gridboxes. The apparent convective momentum source deduced using the coarse-graining technique has a much broader pdf than that found in the forecast model. It suggests a more active role for convective momentum transport than that achieved by the convective parametrization scheme (assuming that the CRM simulation is sufficiently realistic).

A way of addressing the representation of unpredictable fluctuations in convective fluxes at the scale of NWP model grids is to use the deduced pdfs as a basis for modulation of the computed parametrized fluxes. Using a cellular automaton as a pattern generator, an example is presented of the effects of such parametrized tendency modulation using the CRM model run at coarse resolution with a convective parametrization scheme. It is shown that some modest improvement in the character of the precipitation and 850 mb zonal wind fields (judged from Hovmuller diagrams of the corresponding cloud-resolving run) can be obtained by such a technique.

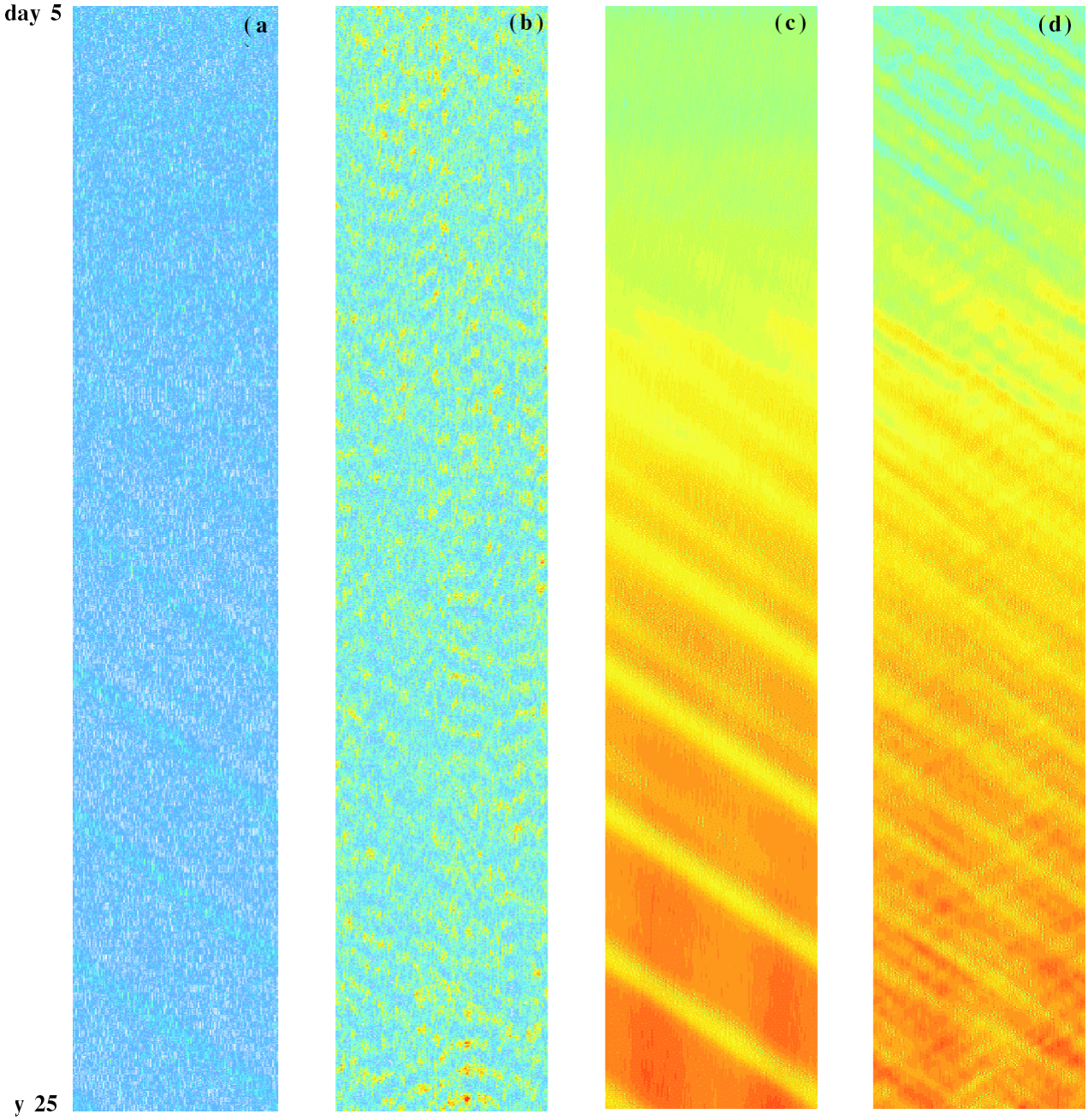

Figure 18 Hovmuller diagrams of surface rainfall rate ((a) and (b)) and 850 mb u ((c) and (d)) using the CRM model with dx=32 km and dy=40 km together with a convective parametrization scheme. Figs. (b) and (d) show the effect of stochastically-perturbing the temperature and humidity tendencies from the parametrization scheme. Time runs downwards and the horizontal scale represents $0 \le x \le 8192$ *km. Precipitation rate ranges from zero (white) to 15 mm/day (red) and* u *ranges from -15 m/s (white) to zero (red). The time period shown is between days 5 and 25.*

From an operational NWP perspective, many technical and implementation issues are associated with adapting convective parametrization schemes to accommodate statistical fluctuations. Even without explicit stochastic terms, current parametrization schemes are complex, highly tuned and sensitive to the choice of numerical advection algorithm and diffusion. Leaving aside the difficult gridpoint storm issue, the time variation of gridpoint convective tendencies may exhibit chaotic fluctuations due in part to poor numerical implementation. The development of stochastic convective parametrizations cannot therefore be carried out without addressing the same difficult issues that blight the 'deterministic' parametrization problem.

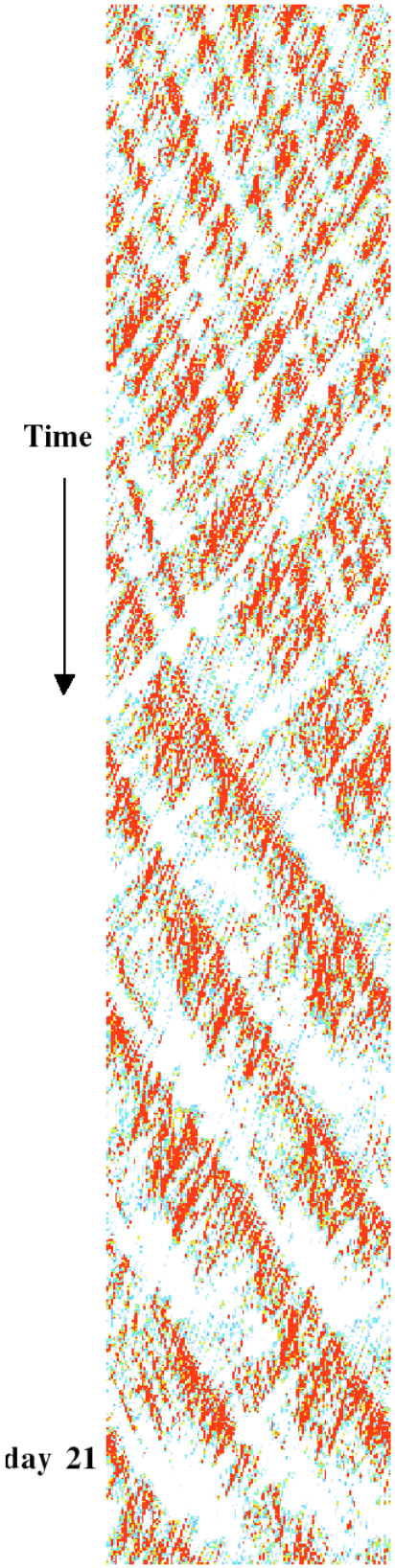

Figure 19 Hovmuller diagram of surface precipitation rate from the zonally symmetric SST run with $\Delta x = 1\,km$ *coarse-grain averaged to boxes of width 32 km (for comparison with Figures 18 (a) and (b)). The scales and colour intensity are the same as in Figure 18. (Figure 6 represents the same case without coarse-graining and with a different colour scale).*

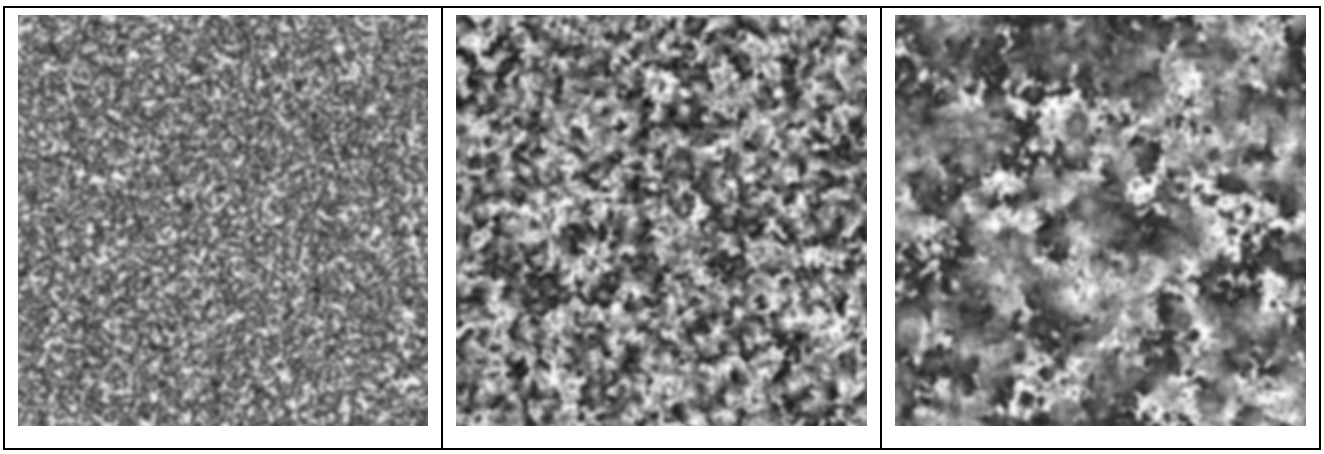

Figure 20 Weighting functions derived from the CA for three different choices of the number of lives allocated initially to new cells (left) 10; (middle) 50, and (right) 100. The increasing scale of the CA patterns with number-of-lives could be used to make the scale of stochastic fluctuations a function of a local model parameter like CAPE.

Acknowledgments

Special thanks go to Peter Bechtold for supplying the convective parametrization scheme and the data for the pdfs from the IFS, together with much useful practical advice. Peter Janssen pointed out the deficiencies of the IFS kinetic energy spectrum to us and we thank him, Martin Miller, Anton Beljaars, Adrian Tompkins, Brian Hoskins, and Leon Hermanston for many helpful discussions.

References

Bechtold, P., Bazile, E. Guichard, F., Mascart, P. and Richard, E. (2001) A mass flux convection scheme for regional and global models. *Q.J.R. Meteorol. Soc*., **127**, 869-886.

Buizza, R. and Miller, M. and Palmer, T.N. (1999) Stochastic representation of model uncertainties in the ECMWF Ensemble Prediction System. *Q.J.R. Meteorol. Soc*., **125**, 2887-2908.

Grabowski, W.W. and Moncrieff, M.W. (2001) Large-scale organization of tropical convection in two-dimensional explicit numerical simulations. *Q.J.R. Meteorol. Soc.*,127,445-468.

Hamilton, K. (1998) Dynamics of the tropical middle atmosphere : a tutorial review. *Atmosphere-Ocean*, **36,** 319-354.

Khouider, B., Majda, A.J. and Katsoulakis, M.A. (2003) Coarse-grained stochastic models for tropical convection and climate. *Proc. Nat. Acad, Sci*., **100,** 11941-11946.

Leonard, B.P., MacVean, M.K. and Lock, A.P. (1993) Positivity-preserving numerical schemes for multidimensional advection. *Comput. Methods Appl. Mech. Eng.,* **19**, 59-98.

Mason, P.J. and Thomson, D. (1992) Stochastic backscatter in large-eddy simulations of boundary layers. *J. Fluid Mechs.*, **242**, 51-78.

Nastrom, G.D. and Gage, K.S. (1985) A climatology of atmospheric wavenumber spectra of wind and temperature observed by commercial aircraft. *J. Atmos. Sci*., 42, 950-960

Piacsek, S.A. and Williams, G.P. (1970) Conservation properties and convective difference schemes. *J. Comput. Phys*., **6**, 392-405.

Palmer,T.N. (2001) A nonlinear dynamical perspective on model error : a proposal for non-local stochastic-dynamic parametrization in weather and climate prediction models. *Q.J.R. Meteorol. Soc.*,127, 279-304.

Shutts, G.J. and Gray, M.E.B. (1994) A numerical modeling study of the geostrophic adjustment process following deep convection. *Q.J.R. Meteorol. Soc*., **120**, 1145-1178.

Wolfram, S. (2002) A New Kind of Science. *Wolfram Media Inc.,* 1197 pp.